Variation of anomalous Pr ordering and crystal symmetry for the oxygenated $Pr_{1+x}Ba_{2-x}Cu_3O_{7+y}$ system

H. M. Luo, B. N. Lin, Y. H. Lin, H. C. Chiang, Y. Y. Hsu, T. I. Hsu, T. J. Lee, and H. C. Ku
Department of Physics, National Tsing Hua University, Hsinchu 300, Taiwan

C. H. Lin and H.-C. I. Kao
Department of Chemistry, Tamkang University, Tamsui 251, Taiwan

J. B. Shi
Department of Electronic Engineering, Feng Chia University, Taichung 407, Taiwan

J. C. Ho
Department of Physics, Wichita State University, Wichita, Kansas 67208

C. H. Chang, S. R. Hwang, and W.-H. Li
Department of Physics, National Central University, Chungli 320, Taiwan
(Received 18 November 1999)

Structural, transport, magnetic, calorimetric, and neutron data were reported for the oxygen-annealed $Pr_{1+x}Ba_{2-x}Cu_3O_{7+y}$ or 1212-type $Cu(Ba_{2-x}Pr_x)PrCu_2O_{7+y}$ system ($0 \leqslant x \leqslant 1$, $-0.11 \leqslant y \leqslant 0.31$). Powder x-ray Rietveld analysis indicates that due to subtle oxygen distribution in the CuO_{1+y} plane for these oxygenated cuprates, two structural symmetry transitions were observed, from orthorhombic 1212*C* (CuO chain) O(I) phase (space group *Pmmm*) for $0 \leqslant x \leqslant 0.4$, to tetragonal 1212 *T* phase ($P4/mmm$) for $0.4 \leqslant x \leqslant 0.65$, and then to a different type of orthorhombic 1212 O(II) phase (*Cmmm*) for $0.65 < x < 1$. Resistivity data indicate that Pr-in-Ba is not favorable for metallic state and no superconductivity can be detected for these insulating cuprates. Magnetic-susceptibility, heat-capacity, and neutron-diffraction data show that, regardless of the structural transitions, the anomalous Néel temperature $T_N(\mathrm{Pr})$ decreases monotonically and smoothly from 18 K for $x=0$ to 2.5 K for $x=0.8$, with the same *c*-axis antiferromagnetic Pr spin alignment. The increasing Pr-O bond length observed with decreasing $T_N(\mathrm{Pr})$ indicates that this unusual Pr magnetic ordering is closely correlated with the wave-function overlap between Pr-4*f* orbital and eight O-$2p_\pi$ orbital in the CuO_2 bilayer.

I. INTRODUCTION

Superconductivity with T_c above 90 K was observed for most orthorhombic 123 $R\mathrm{Ba_2Cu_3O_7}$ or 1212*C* (when written as $\mathrm{CuBa_2}R\mathrm{Cu_2O_7}$ to emphasize the CuO_2 bilayers and CuO chain) rare-earth cuprates ($R=$ Y, La, Nd, Sm, Eu, Gd, Dy, Ho, Er, Tm, Yb, or Lu), except for semiconducting $\mathrm{PrBa_2Cu_3O_7}$, where Cu^{2+} magnetic moments ordered antiferromagnetically with Néel temperature $T_N(\mathrm{Cu})$ above room temperature and Pr^{3+} moments ordered with high $T_N(\mathrm{Pr})$ of 17 K.[1–5] The anomalous high $T_N(\mathrm{Pr})$, observed in $\mathrm{PrBa_2Cu_3O_7}$ as well as in other Pr-1212 compounds, $MA_2\mathrm{PrCu_2O_7}$ ($M=$ Hg, Tl, Pb/Cu, Nb; $A=$ Sr, Ba),[6] is much higher than other magnetic rare-earth compounds with a maximum $T_N(R)$ of 2.2 K for superconducting $\mathrm{GdBa_2Cu_3O_7}$.[7] The absence of superconductivity in $\mathrm{PrBa_2Cu_3O_7}$ remains one of the most intriguing puzzles where mechanisms such as hole localization (trapping), hole filling, or magnetic pair breaking have been proposed based on strong wave-function hybridization between Pr $4f$ orbital and O $2p_\pi$ orbital in the CuO_2 bilayer.[5,6,8] However, indications of inhomogeneous superconductivity around 90 K in $\mathrm{PrBa_2Cu_3O_7}$ were reported recently in some low-temperature pulsed-laser deposited thin films, low oxygen-pressure prepared powders or oxygen-annealed traveling-solvent floating-zone grown single crystals.[9–12] These results are in sharp contrast to earlier works and detailed study is thus necessary to clarify this puzzle.

One of the plausible arguments for the appearance of inhomogeneous superconducting $\mathrm{PrBa_2Cu_3O_7}$ samples is that the metastable metallic phase (precondition for superconductivity) is barely stable only near the stoichiometric composition Pr:Ba=1:2 without any or very few Pr partial-substitution in the Ba site which results with long *c*-axis lattice parameter.[9–12] It is well known that due to smaller rare-earth R^{3+} ionic radius as compared with larger Ba^{2+} ionic radius of 0.134 nm, lighter and larger rare-earth R^{3+} ions are very easily incorporated into the Ba sites to form a wide range of solid solutions with the formula $R_{1+x}\mathrm{Ba}_{2-x}\mathrm{Cu_3O}_{7+y}$ or $R(\mathrm{Ba}_{2-x}R_x)\mathrm{Cu_3O}_{7+y}$ ($R=$ La, Pr, Nd, Sm, or Eu).[13–27] For the $Pr_{1+x}Ba_{2-x}Cu_3O_{7+y}$ system,[14–21] nearly single phase compounds up to $x \sim 0.7$ were reported, but with conflicting reports on the variation of oxygen parameter *y*, crystal structure, as well as Pr ordering due to different sample preparation conditions. However, a study on the isostructural $Nd_{1+x}Ba_{2-x}Cu_3O_{7+y}$ system indicated that the single phase region with complex structural variation can be extended up to $x \sim 1$ using various oxygen annealing temperatures,[24–26] and the often-neglected oxygen

parameter y plays a crucial role on both the variation of crystal symmetry and physical properties.

In this paper, through careful material control and sample preparation, we have successfully extended the single phase limit of the oxygenated $Pr_{1+x}Ba_{2-x}Cu_3O_{7+y}$ solid solution up to $x\sim 1$, and through various measurement techniques, we are able to study the complex interplay between crystal symmetry, unusual magnetic property, and unconventional superconductivity in this system.

II. EXPERIMENT

The oxygenated samples with nominal composition $Pr_{1+x}Ba_{2-x}Cu_3O_{7+y}$ ($0\leqslant x\leqslant 1$) were synthesized by solid-state reaction using high-purity Pr_6O_{11} (99.99%), $BaCO_3$ (99.999%), and CuO (99.99%) powders. Samples were thoroughly mixed and carefully calcined between 850 and 910 °C in air for 2 days with several intermediate regrindings. The calcined powder was then pressed into pellets and were sintered in flowing Ar gas at 900–940 °C for 1 day in order to prevent the formation of unwanted magnetic impurity phase $PrBaO_3$. Finally, these samples were annealed in flowing O_2 gas at 400 °C for 1 day to ensure the desired oxygen content,[26,28] then slowly furnace cooled to room temperature. The oxygen content parameter y was determined from precision iodometric titration method.[29]

The powder x-ray Rietveld analysis data were collected with a Rigaku Rotaflex 18-kW rotating anode diffractometer using graphite monochromatized Cu-K_α radiation with a scanning step of 0.02° (10-sec counting time per step) in the 2θ range of 20–120°. A RIQAS refinement program was used with inorganic crystal structure database (ICSD) and diffraction database (ICDD).[30]

The electrical resistivity data were obtained using the standard low-frequency ac technique from 15 to 300 K in a closed cycle refrigerator with Si-diode thermometry. The dc magnetic-susceptibility measurements were carried out with a Quantum Design MPMS or a μ-metal shielded $MPMS_2$ superconducting quantum interference device (SQUID) magnetometer in various applied magnetic field from 2 to 350 K. The low-temperature (4–20 K) specific-heat measurements were made in an adiabatic calorimeter with pulsed heating and Ge thermometry.

Neutron-diffraction measurements were performed at the Research Reactor at the U. S. National Institute of Standards and Technology. The data were collected using the BT-9 triple axis spectrometer operated in double-axis mode. A pyrolytic graphic PG(002) crystal was used to extract neutrons of energy 14.8 meV (0.2359 nm). A PG filter was also employed to suppress higher-order wavelength contamination, and the angular collimations used were 60′-40′-40′. Powder sample was mounted in a cylindrical Al can, and a pumped ^{4}He cryostat was used to cool the sample.

III. RESULTS AND DISCUSSION

A. Crystal symmetry variation

For the 400 °C oxygenated $Pr_{1+x}Ba_{2-x}Cu_3O_{7+y}$ or 1212-type $Cu(Ba_{2-x}Pr_x)PrCu_2O_{7+y}$ samples with Ar gas presintering, single-phase 1212 compounds can be obtained nearly up to $x=1$ as shown in the powder x-ray-diffraction patterns

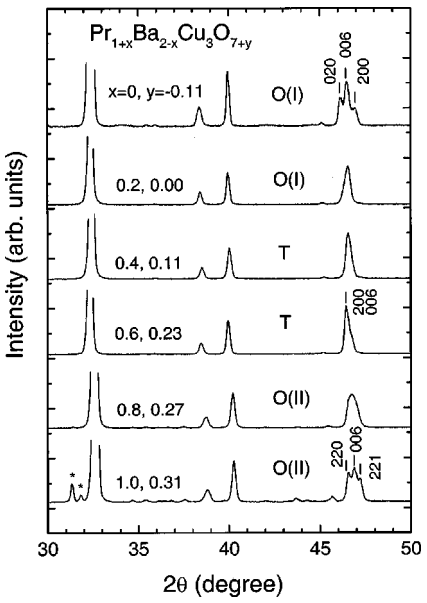

FIG. 1. Powder x-ray-diffraction patterns for six oxygenated $Pr_{1+x}Ba_{2-x}Cu_3O_{7+y}$ samples ($x=0$, 0.2, 0.4, 0.6, 0.8, and 1.0).

in Fig. 1 for six typical samples ($x=0$, 0.2, 0.4, 0.6, 0.8, and 1.0, with oxygen parameter y determined from precision iodometric titration). Two phase transitions were observed for this oxygenated system. The 1212C orthorhombic structure (denoted as O(I) phase) persists only for $x=0$ and 0.2 samples with splitting (020) and (200) Bragg diffraction lines (with lattice parameters $a_0<b_0\sim 0.39\,\text{nm}\sim c_0/3$). For $x=0.4$ and 0.6 samples, single (200) diffraction peak, which is accidentally close to the (006) line, indicates a phase transition from the orthorhombic O(I) phase to a 1212 tetragonal phase (denoted as T phase, with $a_t=b_t\sim 0.39\,\text{nm}>c_t/3$). For $x=0.8$ and 1.0 samples, a further phase transition from the T phase to a different 1212 orthorhombic phase occurs [denoted as O(II)], with larger lattice parameters $a_0<b_0\sim 0.55\,\text{nm}\sim\sqrt{2}a_t$. Small amount of impurity phases observed for $x=1.0$ near 31–32° indicates the solubility limit of smaller Pr in Ba site. The variation of O(I)-T-O(II) orthorhombic/tetragonal lattice parameters a, b, c, oxygen parameter y, as well as phase boundaries for the oxygenated $Pr_{1+x}Ba_{2-x}Cu_3O_{7+y}$ system are shown in Fig. 2. For these

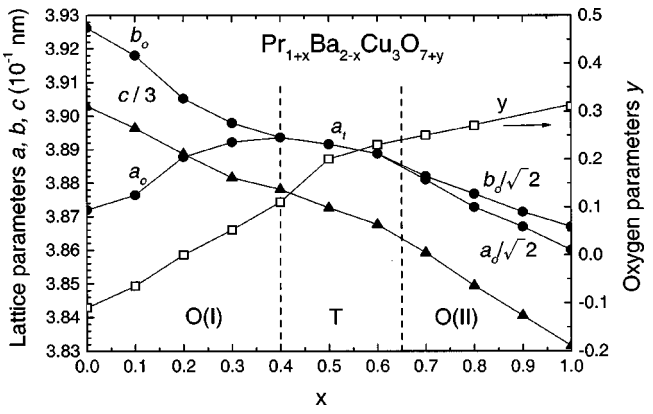

FIG. 2. Variation of orthorhombic/tetragonal lattice parameters a, b, c, oxygen parameter y and O(I)-T-O(II) phase boundaries for the oxygenated $Pr_{1+x}Ba_{2-x}Cu_3O_{7+y}$ system.

TABLE I. Structural parameters of orthorhombic 1212*C* O(I)-phase $Pr_{1.2}Ba_{1.8}Cu_3O_{7.0}$.

Space group: *Pmmmm* (No. 47), $Z=1$
Cell parameters: $a=0.388\,79(3)$, $b=0.390\,52(3)$, $c=1.166\,61(9)$ nm, $V=0.177\,13(1)$ nm^3; $d=6.740$ g/cm^3.

Atom	Position	x	y	z	Occupancy	B_{iso} (nm^2)
Pr	1*h*	1/2	1/2	1/2	1	0.0020
Ba/Pr	2*t*	1/2	1/2	0.1818	0.9/0.1	0.0035
Cu(1)	2*q*	0	0	0.3511	1	0.0043
Cu(2)	1*a*	0	0	0	1	0.0046
O(1)	2*r*	0	1/2	0.3716	1	0.01
O(2)	2*s*	1/2	0	0.3745	1	0.01
O(3)	2*q*	0	0	0.1651	1	0.01
O(4)	1*e*	0	1/2	0	0.7	0.01
O(5)	1*b*	1/2	0	0	0.3	0.01

R factors: $R_p=3.43\%$ (20–120°), $R_{wp}=5.09\%$, $R_B=2.56\%$ (381 reflections).

Selected interatomic distances (nm) and bond angle:

Pr-O(1)	0.245 41	Pr-O(1)-Pr	104.8°
Pr-O(2)	0.244 05	Pr-O(2)-Pr	106.3°
Pr-Cu(1)	0.325 72	Cu(1)-O(1)-Cu(1)	162.4°
Pr-Pr	0.388 79, 0.390 52	Cu(1)-O(2)-Cu(1)	168.2°
Cu(1)-O(1)	0.196 72		
Cu(1)-O(2)	0.196 30		
Ba/Pr-O(1)	0.294 65		
Ba/Pr-O(2)	0.297 77		
Ba/Pr-O(3)	0.276 22		

TABLE II. Structural parameters of tetragonal 1212 *T*-phase $Pr_{1.5}Ba_{1.5}Cu_37.2$.

Space group: *P*4/*mmm* (No. 123), $Z=1$.
Cell parameters: $a=0.389\,16(3)$ nm, $c=1.161\,77(9)$ nm, $V=0.175\,95(1)$ nm^3; $d=6.809$ g/cm^3.

Atom	Position	x	y	z	Occupancy	B_{iso} (nm^2)
Pr	1*d*	1/2	1/2	1/2	1	0.0020
Ba/Pr	2*h*	1/2	1/2	0.1800	0.75/0.25	0.0035
Cu(1)	2*g*	0	0	0.3497	1	0.0043
Cu(2)	1*a*	0	0	0	1	0.0046
O(1)	4*i*	0	1/2	0.3706	1	0.01
O(2)	2 *f*	0	1/2	0	0.6	0.01
O(3)	2*g*	0	0	0.1626	1	0.01

R factors: $R_p=3.48\%$ (20–120°), $R_{wp}=4.20\%$, $R_B=4.71\%$ (227 reflections).

Selected interatomic distances (nm) and bond angle:

Pr-O(1)	0.245 89	Pr-O(1)-Pr	104.6°
Pr-Cu(1)	0.325 90	Cu(1)-O(1)-Cu(1)	165.8°
Pr-Pr	0.389 16		
Cu(1)-O(1)	0.196 09		
Ba/Pr-O(1)	0.294 78		
Ba/Pr-O(3)	0.275 92		

400 °C oxygen annealed samples, the oxygen content y increases monotonically with x from $y=-0.11$ for $x=0$ ($PrBa_2Cu_3O_{6.89}$) to $y=0.31$ for $x=1$ ($Pr_2BaCu_3O_{7.31}$). The Pr-1237 or 1212*C*-type orthorhombic O(I) phase (space group *Pmmm*) persists up to $x=0.4$, then transfers to the Pr-1236 or $TlBa_2CaCu_2O_7$ 1212-type tetragonal *T* phase (space group *P*4/*mmm*). For $x>0.65$, a different type of 1212 orthorhombic O(II) phase with twice the unit-cell volume ($V_0\sim 2\ V_t$) was observed. It is noted that, regardless of the structural change, the *c*-axis lattice parameter *c* and unit-cell volume *V* (or *V*/2 for O(II) phase) decrease monotonically with increasing smaller Pr^{3+} (ionic radius 0.1013 nm) partial substitution for larger Ba^{2+} ion (0.134 nm). The *c* parameter decreases from 1.1709 nm for $x=0$ to 1.1666 nm for $x=0.2$, 1.1618 nm for $x=0.5$, 1.1578 nm for $x=0.7$, and 1.149 48 nm for $x=1$.

The room-temperature powder x-ray Rietveld structural refinements were performed to all samples investigated. The refined structural parameters of three typical samples: O(I)-phase $Pr_{1.2}Ba_{1.8}Cu_3O_{7.0}$ with space group *Pmmm*,[31] *T*-phase $Pr_{1.5}Ba_{1.5}Cu_3O_{7.2}$ with space group *P*4/*mmm*,[21,31] and O(II)-phase $Pr_{1.7}Ba_{1.3}Cu_3O_{7.25}$ with space group *Cmmm* are listed in Tables I, II, and III, respectively. The oxygen content parameter *y* determined from iodometric titration was taken as a fixed value in the refinement process. The powder x-ray refinement patterns for the O(II)-phase compound $Pr_{1.7}Ba_{1.3}Cu_3O_{7.25}$ are shown in Fig. 3 with satisfied *R* factors of $R_p=5.72\%$ (20–120° pattern), $R_{wp}=6.78\%$ (weighted pattern), and $R_B=5.07\%$ (345 Bragg reflection lines). Some selected interatomic distances and bond angle are also listed in Tables I–III for further discussion. Room-temperature neutron powder Rietveld refinements on O(I)-phase (*x*

TABLE III. Structural parameters of orthorhombic 1212 O(II) $Pr_{1.7}Ba_{1.3}Cu_3O_{7.25}$.

Space group: *Cmmm* (No. 65), $Z=2$.
Cell parameter: $a=0.548\,85(3)$, $b=0.549\,00(3)$, $c=1.157\,75(9)$ nm, $V=0.348\,85(1)$ nm^3; $d=6.904$ g/cm^3.

Atom	Position	x	y	z	Occupancy	B_{iso} (nm^2)
Pr	2*c*	1/2	0	1/2	1	0.0020
Ba/Pr	4*l*	0	1/2	0.1803	0.65/0.35	0.0035
Cu(1)	4*k*	0	0	0.3501	1	0.0043
Cu(2)	2*a*	0	0	0	1	0.0046
O(1)	8*m*	1/4	1/4	0.3681	1	0.01
O(2)	8*p*	0.2530	0.2519	0	0.313	0.01
O(3)	4*k*	0	0	0.1649	1	0.01

R factors: $R_p=5.72\%$ (20–120°), $R_{wp}=6.78\%$, $R_B=5.07\%$ (345 reflections).

Selected interatomic distances (nm) and bond angle:

Pr-O(1)	0.246 95	Pr-O(1)-Pr	103.6°
Pr-Cu(1)	0.324 70	Cu(1)-O(1)-Cu(1)	167.7°
Pr-Pr	0.388 15		
Cu(1)-O(1)	0.195 19		
Ba/Pr-O(1)	0.291 44		
Ba/Pr-O(3)	0.275 08		

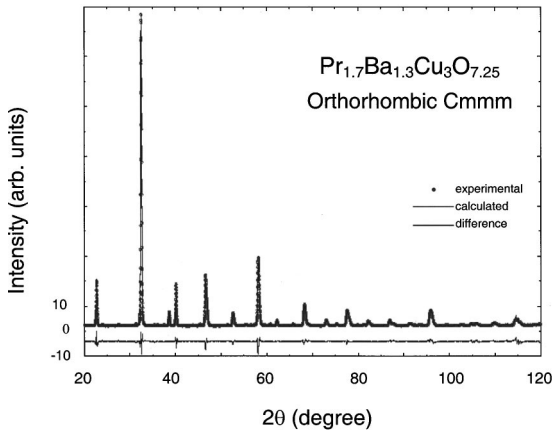

FIG. 3. Experimental (dotted), calculated (curve), and difference of the powder x-ray-diffraction patterns for the O(II)-phase compound $Pr_{1.7}Ba_{1.3}Cu_3O_{7.25}$.

$=0.2$) and *T*-phase ($x=0.5$) samples give similar results and comparable *R* factors with oxygen content parameter *y* in the refinement process.

Figure 4 shows the schematic structure of 1212*C* O(I) phase ($0\leqslant x<0.4$), 1212 *T* phase ($0.4\leqslant x\leqslant 0.65$), and 1212 O(II) phase ($0.65<x<1$). These three structures are in fact very similar and the only major difference is due to the oxygen distribution in the CuO_{1+y} plane as shown in Fig. 5. The 1212-type $Cu(Ba_{2-x}Pr_x)PrCu_2O_{7+y}$ cuprates consist of two fully occupied CuO_2 layers and one partially oxygen occupied CuO_{1+y} plane. The oxygen content parameter *y* is controlled by both oxygen annealing temperature (400 °C in our case) and the amount of smaller Pr^{3+} ions in larger Ba^{2+} site. Contracted (Ba,Pr)-O layer tend to introduce more oxygen into the adjacent partially occupied CuO_{1+y} plane. For the 1212*C* O(I) phase, uneven oxygen distribution in the CuO_{1+y} plane results in the well-known orthorhombic chain-like structure. The progressive substitution of Ba^{2+} by Pr^{3+} ions increases the oxygen content in the CuO_{1+y} plane, which makes it difficult to keep uneven oxygen distribution in the CuO_{1+y}, and results in the disappearance of the orthorhombicity for $x>0.4$. In fact, as in the isostructural $Nd_{1+x}Ba_{2-x}Cu_3O_{7+y}$ system,[24–26] the oxygen annealing at

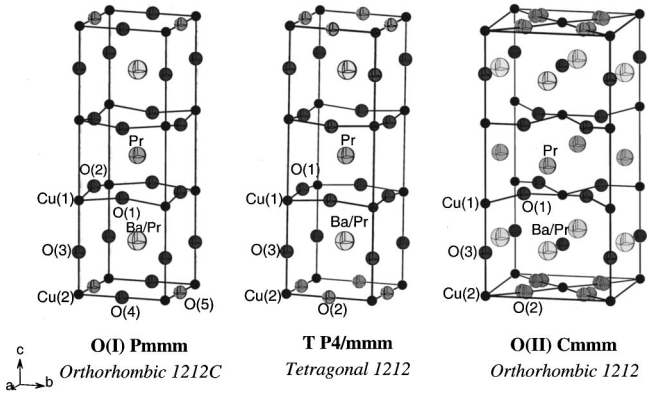

FIG. 4. Schematic representation of orthorhombic 1212*C* O(I) phase (*Pmmm*, $0\leqslant x<0.4$), tetragonal 1212 *T* phase (*P*4/*mmm*, $0.4\leqslant x\leqslant 0.65$), and orthorhombic 1212 O(II) phase (*Cmmm*, $0.65<x<1$) in the oxygenated $Pr_{1+x}Ba_{2-x}Cu_3O_{7+y}$ system.

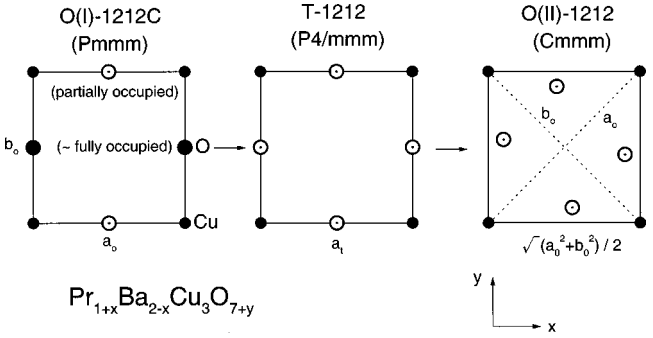

FIG. 5. Correlation between crystal symmetry O(I)-*T*-O(II) and oxygen distribution in the CuO_{1+y} plane for the oxygenated $Pr_{1+x}Ba_{2-x}Cu_3O_{7+y}$ system.

low temperature is extremely important to maintain the orthorhombicity for smaller *x*-value samples. The *T* phase is best represented by the $Pr_{1.5}Ba_{1.5}Cu_3O_{7.2}$ composition, which was sometimes written as $Pr_3Ba_3Cu_6O_{14.4}$ (336-type phase). The phase transition to the O(II) phase for $x>0.65$ may be due to the displacement of oxygen from the ideal oxygen position in the CuO_{1+y} plane, and is sometimes denoted as the 213 phase (for the $Pr_2BaCu_3O_{7.31}$ composition). This structure is very similar to the orthorhombic 2212 $Bi_2Sr_2CaCu_2O_{8+\delta}$ structure where $Bi_2O_{2+\delta}$ biplane is replaced by single CuO_{1+y} plane and similar oxygen arrangement in the CuO_{1+y} plane were used in Table III and shown in Fig. 5.[31]

B. Physical property variation

The temperature dependence of electrical resistivity $\rho(T)$ for parent compound $PrBa_2Cu_3O_{6.89}$, O(I)-phase $Pr_{1.2}Ba_{1.8}Cu_3O_{7.0}$, and *T*-phase $Pr_{1.5}Ba_{1.5}Cu_3O_{7.2}$ are shown collectively in Fig. 6. Transport data show that all samples exhibit semiconducting or insulating behavior with room-temperature resistivity ρ_{RT} of 34 mΩ cm for $x=0$, 54 mΩ cm for $x=0.2$, and 456 mΩ cm for $x=0.5$. No superconductivity can be observed for all three compounds. The insulating behavior for the tetragonal $Pr_{1.5}Ba_{1.5}Cu_3O_{7.2}$ sample with high resistivity of $\rho(70\,K)\sim 9.2\,k\Omega$ cm is not really surprising since all 1212 tetragonal rare-earth cuprates $RBa_2Cu_3O_6$ or $MA_2RCu_2O_7$ (R=rare earths; M=Hg, Tl, Pb/Cu, Nb; *A*

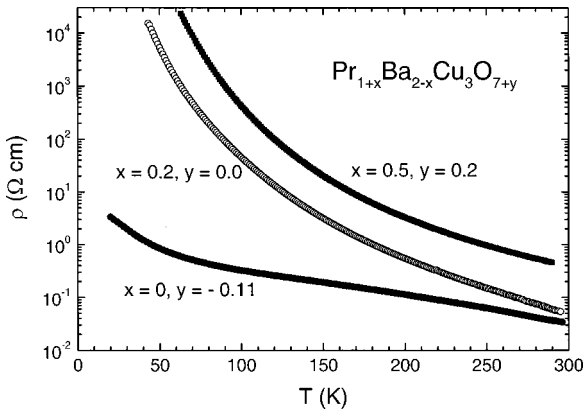

FIG. 6. Logarithmic temperature dependence of electrical resistivity $\rho(T)$ for three typical oxygenated samples $Pr_{1+x}Ba_{2-x}Cu_3O_{7+y}$ ($x=0$, 0.2, and 0.5).

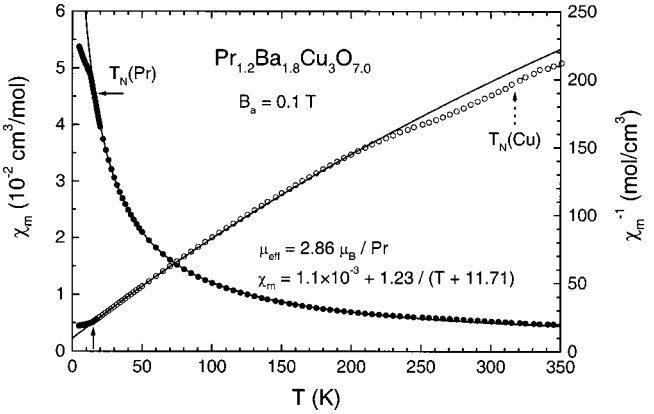

FIG. 7. Temperature dependence of molar magnetic susceptibility $\chi_m(T)$ and inverse susceptibility $\chi_m^{-1}(T)$ in 0.1-T field for O(I)-phase sample $Pr_{1.2}Ba_{1.8}Cu_3O_{7.0}$.

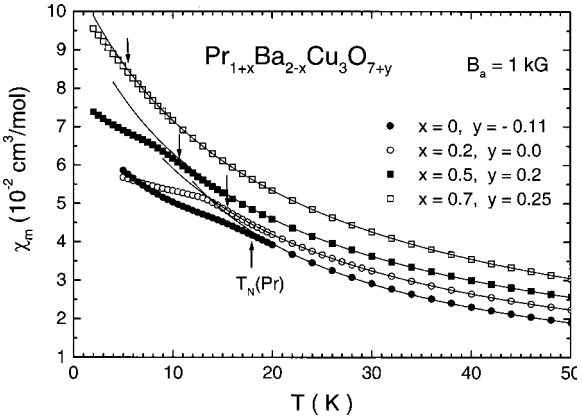

FIG. 8. Low-temperature magnetic susceptibility $\chi_m(T)$ for four typical oxygenated samples ($x=0$, 0.2, 0.5, and 0.7).

=Sr, Ba) are insulators.[6] However, it is surprising that even for the orthorhombic $Pr_{1.2}Ba_{1.8}Cu_3O_{7.0}$ sample, high resistivity of $\rho(50\ \mathrm{K})$ of 5.3 $k\Omega\,cm$ was observed as compared with $\rho(50\ \mathrm{K})$ of 849 $m\Omega\,cm$ for nonsubstituted compound $PrBa_2Cu_3O_{6.89}$. This shows the serious effect of hole depletion due to Pr^{3+} antidoping and supports the assumption that hole delocalization in the stoichiometric and fully oxygenated composition Pr:Ba:Cu:O=1:2:3:7 may be essential for the occurrence of possible metallic superconducting state.[9–12]

The temperature dependence of molar magnetic susceptibility $\chi_m(T)$ and inverse susceptibility $\chi_m^{-1}(T)$ for insulating O(I)-phase $Pr_{1.2}Ba_{1.8}Cu_3O_{7.0}$ sample in an applied field of 0.1 T is shown in Fig. 7. Below 250 K, the data can be well fitted by a Curie-Weiss law $\chi_m(T)=\chi_0+C/(T-\theta_p)$ (solid line), with a negative paramagnetic intercept θ_p of -11.7 K and an effective magnetic moment μ_{eff} of $2.86\mu_B$ per Pr ion, if the small saturation Cu moments of $\sim 0.3-0.5\mu_B$ can be neglected. The high-temperature deviation indicates that Cu moments ordered around T_N(Cu) of 320–330 K. The low-temperature deviation indicates that Pr^{3+} moments are ordered antiferromagnetically around T_N(Pr) of 15.5 K, which is better determined from the minimum of derivative $d\chi_m/dT$. Although 20% more Pr^{3+} ions are incorporated into the compound, these extra moments make no contribution for T_N(Pr) ordering due to the random and dilute distribution of Pr in Ba matrix with longer $(Pr_{0.1}/Ba_{0.9})$-O(1)/O(2)/O(3) bond lengths of 0.276–0.298 nm, as compared to shorter Pr-O(1)/O(2) bond lengths of 0.244–0.245 nm between Pr and CuO_2 bilayer (see Table I).

Low-temperature magnetic susceptibility $\chi_m(T)$ for four typical samples ($x=0$, 0.2, 0.5, and 0.7) are shown collectively in Fig. 8, along with the accompanying Curie-Weiss-law fitted lines. The magnitude of magnetic moment increases with increasing magnetic Pr concentration, however, T_N(Pr) as determined from $d\chi_m/dT$ minimum, decreases from 18 K for $PrBa_2Cu_3O_{6.89}$ to 15.5 K for $Pr_{1.2}Ba_{1.8}Cu_3O_{7.0}$, 10.5 K for $Pr_{1.5}Ba_{1.5}Cu_3O_{7.2}$, and 5.5 K for $Pr_{1.7}Ba_{1.3}Cu_3O_{7.25}$. From fitted curves, it was observed that Curie-Weiss intercept θ_p increases from -7.26 K for $x=0$ to -11.7 K for $x=0.2$, -16.1 K for $x=0.5$, and -18.4 K for $x=0.7$. Effective magnetic moment μ_{eff} varying in the range of 2.86 to $3.18\mu_B$/Pr indicates Pr^{3+} nature for these samples.

The low-temperature specific-heat data $C(T)$ for $x=0.2$, 0.5, and 0.7 as shown in Fig. 9 confirm the Pr long-range order with a distinct but broad magnetic transition due to the quasi-two-dimensional (quasi-2D) character of Pr long-range order with very strong in-plane magnetic coupling through strong Pr $4f$-O $2p_\pi$ hybridization and weak c-axis coupling. To help delineate the different contributions to the total heat capacity, the data when replotted as C/T versus T^2 (inset) show the Pr ordering superimposed on a βT^3 lattice contribution as well as an approximately linear term γT. The linear term coefficient γ decreases from 375 mJ/mol K^2 for $x=0.2$ to 355 mJ/mol K^2 for $x=0.5$ and 340 mJ/mol K^2 for $x=0.7$.

Neutron-diffraction patterns were taken at low temperature to study the intensity variation with temperature. Figure 10 shows the {1/2,1/2,1/2} magnetic Bragg reflection at 25.6° that characterizes the appearance of Pr spin antiferromagnetic ordering below $T_N(\mathrm{Pr})\sim 10.5$ K for T-phase sample $Pr_{1.5}Ba_{1.5}Cu_3O_{7.2}$. Inset shows the differences between the diffraction patterns between 24 and 27° taken at $T=1.4$ and 18.5 K (the solid line is a guide to the eye only). The magnetic structure consists of nearest-neighbor spins along all crystallographic directions were antiparallel aligned with spin direction along the c axis. This Pr sublattice magnetic structure is indeed similar to orthorhombic $PrBa_2Cu_3O_7$ and tetragonal $TlBa_2PrCu_2O_7$.[4,6,32]

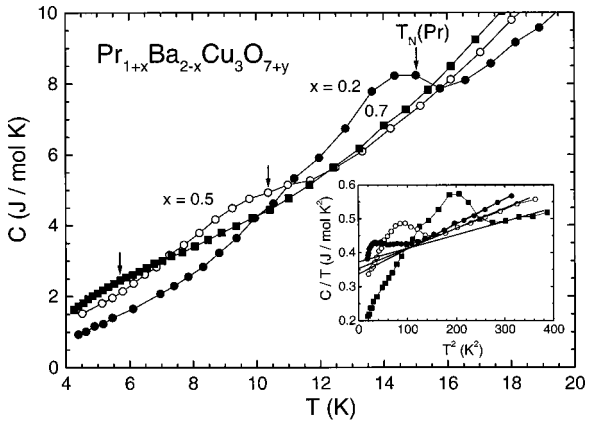

FIG. 9. Low-temperature specific heat $C(T)$ for three typical oxygenated samples ($x=0.2$, 0.5, and 0.7).

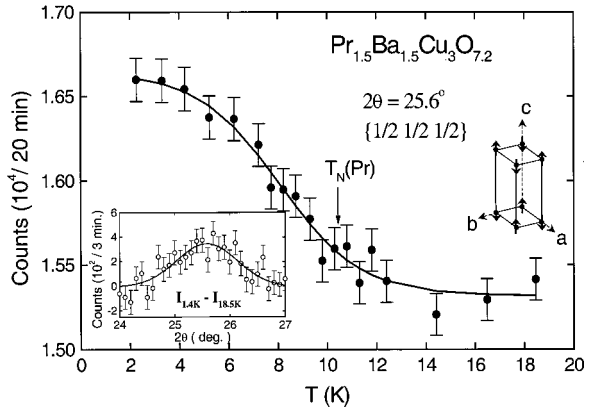

FIG. 10. Temperature dependence of magnetic $\{\frac{1}{2},\frac{1}{2},\frac{1}{2}\}$ diffraction intensity observed for *T*-phase sample $Pr_{1.5}Ba_{1.5}Cu_3O_{7.2}$.

The variation of T_N(Pr) for the oxygenated $Pr_{1+x}Ba_{2-x}Cu_3O_{7+y}$ system is shown in Fig. 11. T_N(Pr) decreases monotonically from 18 K for $x=0$ to 17 K for $x=0.1$, 15.5 K for $x=0.2$, 13.5 K for $x=0.3$, 12 K for $x=0.4$, 10.5 K for $x=0.5$, 8 K for $x=0.6$, 5.5 K for $x=0.7$, and 2.5 K for $x=0.8$. No T_N(Pr) can be detected above 2 K for $x=0.9$ and 1.0. Similar behavior was observed for the isostructural $Pr(Ba_{2-x}La_x)Cu_3O_{7+y}$ system (nonmagnetic La^{3+} in Ba site) with slightly different phase boundaries.[33–35] The monotonically decreasing T_N(Pr) and the insensitiveness of T_N(Pr) to the structural phase transition boundaries suggest the close tie among O(I), *T*, and O(II) phases, and the T_N(Pr) variation is believed to be the direct result of subtle change of wave-function overlap between outerlying light-rare-earth Pr $4f_{z(x^2-y^2)}$ orbital and eight O $2p_\pi$ orbital in the adjacent CuO_2 bilayer. The degree of hybridization can be readily correlated with the Pr-O bond length d(Pr-O). The experimental evidence for the existence of Pr $4f$-O $2p_\pi$ orbital hybridization was reported through the direct observation of directional lobes of charge density from the Pr atom toward oxygen in the CuO_2 bilayer using the maximum entropy method (MEM) charge-density study of synchrotron radiation data.[36]

The Pr-O hybridization bond length d(Pr-O) can be determined accurately through powder x-ray Rietveld refinement analysis as shown in Tables I, II, and III for three typical

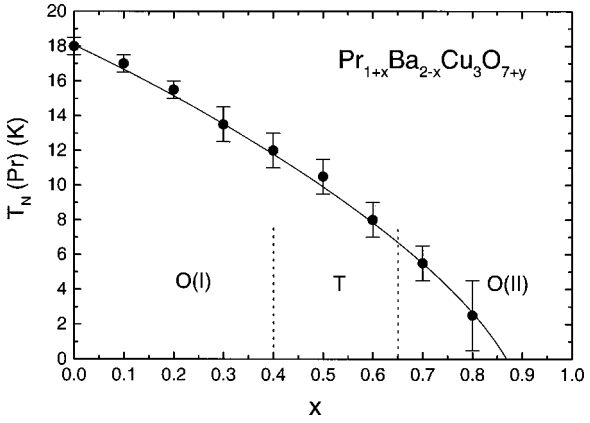

FIG. 11. Variation of T_N(Pr) for the oxygenated $Pr_{1+x}Ba_{2-x}Cu_3O_{7+y}$ system.

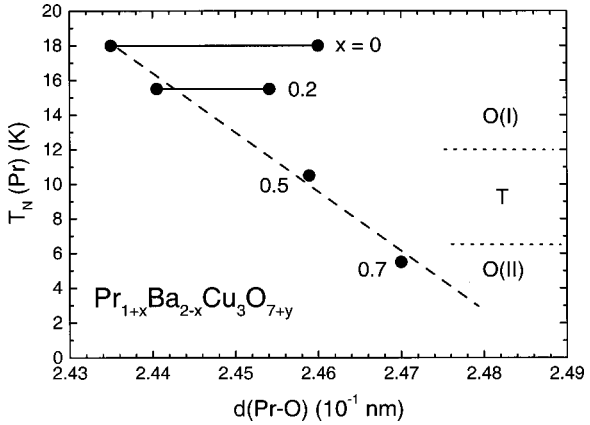

FIG. 12. Correlation between T_N(Pr) and the Pr-O bond length d(Pr-O) in the adjacent CuO_2 bilayer for the oxygenated $Pr_{1+x}Ba_{2-x}Cu_3O_{7+y}$ system.

samples. Slightly different oxygen notations are used in order to unify the notation for three different structures.[31] It was found that, although the unit-cell volume V [$V_o/2$ for O(II) phase] and *c*-axis lattice-parameter decrease with progressive smaller Pr substitution in the Ba site, d(Pr-O) bond length in fact increases with Pr substitution due to the accompanying increasing oxygen content parameter y in the CuO_{1+y} plane. The extra O^{2-} ions pull the (Ba^{2+}/Pr^{3+})-O layers toward the CuO_{1+y} plane, which in turn results with less buckled CuO_2 bilayer (with larger Cu-O-Cu bond angle) and thus longer Pr-O bond length. Figure 12 shows the correlation between T_N(Pr) and Pr-O bond length for the oxygenated $Pr_{1+x}Ba_{2-x}Cu_3O_{7+y}$ system, where T_N(Pr) decreases with increasing Pr-O bond length. In the O(I) phase with two unequal Pr-O bond lengths due to two distinct oxygen sites [denoted as O(1) and O(2) in Table I and Fig. 4] in the CuO_2 bilayer, shorter Pr-O(2) bond length increases from 0.2435 nm for $x=0$ to 0.2441 nm for $x=0.2$. The higher T_N(Pr) for the 1212*C* O(I) cuprates is closely related with the exceptional strong Pr $4f$-O $2p_\pi$ hybridization. For the *T* and O(II) phases with eight equal Pr-O(1) bond lengths [oxygen site denoted as O(1) in Tables II, III, and Fig. 5], d(Pr-O) increases further to 0.2459 nm for $x=0.5$ and 0.2470 nm for $x=0.7$. The increasing Pr-O bond length with decreasing T_N indicates that Pr antiferromagnetic order is closely correlated with Pr $4f$-O $2p_\pi$ orbital hybridization that is essential in the superexchange interaction mechanism. This superexchange interaction is highly anisotropic and the long-range Pr ordering is thus very much quasi-two-dimensional as seen from specific-heat and neutron-diffraction data. The role of Pr-O-Pr bond angle is not quantitatively understood but is certainly involved in the magnetic exchange coupling between Pr and Cu sublattices through Pr $4f_{z(x^2-y^2)}$-O $2p_\pi$ as well as Cu $3d_{x^2-y^2}$-O $2p_\sigma$ orbital hybridization.[36–38]

It is interesting to note that due to Pr-O bond-length variation, T_N(Pr) of 12–18 K for the O(I) samples are comparable to 18 K for O(I)-like 2212*C* compound $PrBa_2Cu_4O_8$.[39] For the *T*-phase samples with T_N(Pr) of 6–12 K are close to 4–10 K reported for tetragonal 1212 compounds $MA_2PrCu_2O_{7+\delta}$ (M=Hg, Tl, Pb/Cu, Cu; A=Sr, Ba) (Refs. 6 and 40–43) [with T_N(Pr) variation with d(Pr-O) shown in Fig. 13], 12 K for more complex tetragonal compound

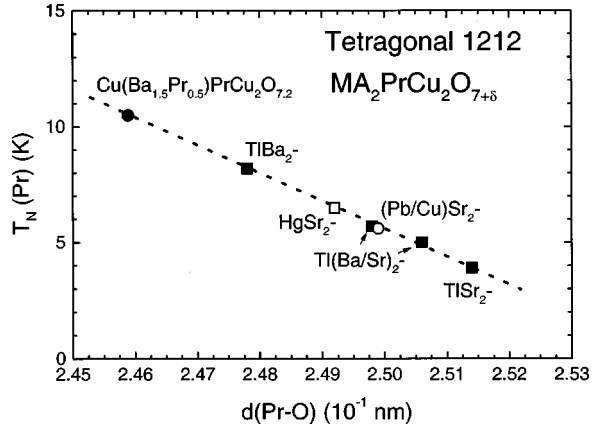

FIG. 13. Variation of T_N(Pr) with Pr-O bond length d(Pr-O) for the tetragonal 1212 compounds $MA_2PrCu_2O_{7+\delta}$ (M=Hg, Tl, Pb/Cu, Cu; A=Sr, Ba, Ba/Pr).

$NbBa_2PrCu_2O_7$,[44] and 9 K for tetragonal 2212 compound $(Pb/Cu)_2(Ba/Sr)_2PrCu_2O_8$.[45] Low T_N(Pr) of 0–6 K for the O(II)-phase samples can be readily compared with no T_N(Pr) observed above 1.4 K for O(II)-phase-like orthorhombic 2212 compound $Bi_2Sr_2PrCu_2O_8$.[6,46]

IV. CONCLUSION

A continuous variation of anomalous Pr antiferromagnetic ordering with T_N(Pr) varying from 18 K for $x=0$ to 2.5 K for $x=0.8$ and below 2 K for $x>0.8$ was observed for the oxygenated $Pr_{1+x}Ba_{2-x}Cu_3O_{7+y}$ system. Regardless the complex structural symmetry change from orthorhombic O(I) phase to tetragonal T and then to orthorhombic O(II) phase, the increasing Pr-O bond lengths between Pr and oxygen in the CuO_2 bilayer with decreasing T_N indicates that the anomalous Pr ordering is closely correlated with strong Pr $4f$-O $2p_\pi$ orbital hybridization. The serious effect of hole-depletion due to Pr^{3+} anti-doping pushes these samples to a more insulating state and prevents any possibility for the occurrence of superconductivity.

ACKNOWLEDGMENTS

The authors are grateful to Professor T. J. Yang of National Chiao-Tung University for helpful discussions. This work was supported by the National Science Council of R.O.C. under Contract Nos. NSC89-2112-M007-023 and -051 (H. C. Ku), M007-052 (T. J. Lee), M008-032 (W. H. Li), M035-006 (J. B. Shi), and 2113-M032-013 (H. -C. I. Kao).

[1] L. Soderholm, K. Zhang, D. G. Hinks, M. A. Beno, J. D. Jorgensen, C. U. Segre, and I. K. Schuller, Nature (London) **328**, 604 (1987).
[2] H. C. Ku, C. C. Chen, and S. W. Hsu, Int. J. Mod. Phys. B **2**, 1411 (1988).
[3] A. Kebede, C. S. Jee, J. Schwegler, J. E. Crow, T. Mihalisin, G. H. Myer, R. E. Salomon, P. Schlottmann, M. V. Kuric, S. H. Bloom, and R. P. Guertin, Phys. Rev. B **40**, 4453 (1989), and references cited therein.
[4] W-H. Li, J. W. Lynn, S. Skanthakumar, T. W. Clinton, A. Kebede, C. S. Jee, J. E. Crow, and T. Mihalisin, Phys. Rev. B **40**, 5300 (1989).
[5] H. B. Radousky, J. Mater. Res. **7**, 1917 (1992), and reference cited therein.
[6] H. C. Ku, Y. Y. Hsu, T. J. Lee, and J. C. Ho, Chin. J. Phys. **36**, 292 (1998), and references cited therein.
[7] J. C. Ho, P. H. Hor, R. L. Meng, C. W. Chu, and C. Y. Huang, Solid State Commun. **63**, 711 (1987).
[8] R. Fehrenbacher and T. M. Rice, Phys. Rev. Lett. **70**, 3471 (1993), and references cited therein.
[9] H. A. Blackstead, J. D. Dow, D. B. Chrisey, J. S. Horwitz, M. A. Black, P. J. McGinn, A. E. Klunzinger, and D. B. Pulling, Phys. Rev. B **54**, 6122 (1996).
[10] Z. Zou, J. Ye, K. Oka, and Y. Nishihara, Phys. Rev. Lett. **80**, 1074 (1998).
[11] K. Oka, Z. Zou, and J. Ye, Physica C **300**, 200 (1998).
[12] J. Ye, Z. Zou, A. Matsushita, K. Oka, Y. Nishihara, and T. Matsumoto, Phys. Rev. B **58**, 619 (1998).
[13] C. U. Segre, B. Dabrowski, D. G. Hinks, K. Zhang, J. D. Jorgensen, M. A. Beno, and I. K. Schuller, Nature (London) **329**, 227 (1987).
[14] B. Okai, M. Kosuge, H. Nozaki, K. Takahashi, and M. Ohta, Jpn. J. Appl. Phys., Part 2 **27**, L41 (1988).
[15] M. Suga, M. Hiratani, and Y. Tarutani (unpublished).
[16] S. K. Malik, S. M. Pattalwar, C. V. Tomy, R. Prasad, N. C. Soni, and K. Adhikary, Phys. Rev. B **46**, 524 (1992).
[17] Y. T. Ren, Y. Y. Xue, Y. Y. Sun, and C. W. Chu, Physica C **213**, 224 (1993).
[18] S. K. Malik, R. Prasad, N. C. Soni, K. Adhikary, and W. B. Yelon, Physica B **223&224**, 562 (1996).
[19] T. B. Lindemer and E. D. Specht, Physica C **268**, 271 (1996).
[20] W. H. Tang and J. Gao, Physica C **315**, 66 (1999).
[21] H. C. Ku, H. M. Luo, Y. P. Chi, B. N. Lin, Y. Y. Hsu, T. J. Lee, J. B. Shi, and H. -C. I. Kao, J. Low Temp. Phys. **117**, 885 (1999).
[22] H. Nozaki, S. Takekawa, and Y. Ishizawa, Jpn. J. Appl. Phys., Part 2 **27**, L31 (1988).
[23] K. Takita, H. Katoh, H. Akinaga, M. Nishino, T. Ishigaki, and H. Asano, Jpn. J. Appl. Phys., Part 2 **27**, L57 (1988).
[24] E. A. Goodilin, N. N. Oleynikov, E. V. Antipov, R. V. Shpanchenko, G. Yu. Popov, V. G. Balakirev, and Yu. D. Tretyakov, Physica C **272**, 65 (1996).
[25] E. Goodilin, M. Kambara, T. Umeda, and Y. Shiohara, Physica C **289**, 37 (1997).
[26] E. Goodilin, M. Limonov, A. Panfilov, N. Khasanova, A. Oka, S. Tajima, and Y. Shiohara, Physica C **300**, 250 (1998).
[27] M. J. Kramer, K. W. Dennis, D. Falzgraf, R. W. McCallum, S. K. Malik, and W. B. Yelon, Phys. Rev. B **56**, 5512 (1997).
[28] M. E. Lopez-Morales, D. Rios-Jara, J. Taguena, R. Escudero, S. La Placa, A. Bezinge, V. Y. Lee, E. M. Engler, and P. M. Grant, Phys. Rev. B **41**, 6655 (1990).
[29] E. H. Appelman, L. R. Morss, A. M. Kini, U. Geiser, A. Umezawa, G. W. Crabtree, and K. D. Carlson, Inorg. Chem. **26**, 3237 (1987).
[30] RIQAS program, Materials Data, Inc., Livermore, CA, 1996.
[31] H. Shaked, P. M. Keane, J. C. Rodriguez, F. F. Owen, R. L.

Hitterman, and J. D. Jorgensen, *Crystal Structures of the High-T_c Superconducting Copper-Oxides* (Elsevier Science, New York, 1994).
[32] W. T. Hsieh, K. J. Chang, W-H. Li, K. C. Lee, J. W. Lynn, C. C. Lai, and H. C. Ku, Phys. Rev. B **49**, 12 200 (1994).
[33] H. C. Ku, H. M. Luo, Y. P. Chi, B. N. Lin, Y. Y. Hsu, C. H. Lin, and H.-C. I. Kao, Physica B (to be published).
[34] R. K. Li, Z. Y. Chen, and Y. T. Qian, Physica C **172**, 335 (1990).
[35] R. Nagarajan, V. Pavate, and C. N. R. Rao, Solid State Commun. **84**, 183 (1992).
[36] M. Takata, T. Takayama, M. Sakata, S. Sasaki, K. Kodama, and M. Sato, Physica C **263**, 340 (1996).
[37] A. T. Boothroyd, A. Longmore, N. H. Andersen, E. Brecht, and Th. Wolf, Phys. Rev. Lett. **78**, 130 (1997).
[38] V. N. Narozhnyi, D. Eckert, K. A. Nenkov, G. Fuchs, T. G. Uvarova, and K. H. Muller, Physica C **312**, 233 (1999).
[39] H. C. Ku, Y. B. You, S. R. Sheen, Y. M. Wan, T. I. Hsu, and Y. Y. Hsu, J. Low Temp. Phys. **105**, 1463 (1996).
[40] C. C. Lai, B. S. Chiou, Y. Y. Chen, J. C. Ho, and H. C. Ku, Physica C **202**, 104 (1992).
[41] C. C. Lai, T. J. Lee, H. K. Fun, H. C. Ku, and J. C. Ho, Phys. Rev. B **50**, 4092 (1994).
[42] H. C. Ku, C. C. Lai, J. H. Shieh, J. W. Liou, C. Y. Wu, and J. C. Ho, Physica B **194-196**, 213 (1994).
[43] C. H. Chou, Y. Y. Hsu, J. H. Shieh, T. J. Lee, H. C. Ku, J. C. Ho, and D. H. Chen, Phys. Rev. B **53**, 6729 (1996).
[44] N. Rosov, J. W. Lynn, H. B. Radousky, M. Bennahmias, T. J. Goodwin, P. Klavins, and R. N. Shelton, Phys. Rev. B **47**, 15 256 (1993).
[45] C. L. Yang, J. H. Shieh, Y. Y. Hsu, H. C. Ku, and J. C. Ho, Phys. Rev. B **52**, 10 452 (1995).
[46] Y. Gao, P. Pernambuco-Wise, J. E. Crow, J. O'Reilly, N. Spencer, H. Chen, and R. E. Salomon, Phys. Rev. B **45**, 7436 (1992).